

# 1 **NO<sub>2</sub>-initiated multiphase oxidation of SO<sub>2</sub> by O<sub>2</sub> on CaCO<sub>3</sub> particles**

2 Ting Yu<sup>\*</sup>, Defeng Zhao<sup>\*,a</sup>, Xiaojuan Song, Tong Zhu

3 BIC-ESAT and SKL-ESPC, College of Environmental Sciences and Engineering, Peking University, Beijing,  
4 100871, China

5 <sup>\*</sup>These authors contributed equally to this work.

6 <sup>a</sup>Now at: Department of Atmospheric and Oceanic Sciences & Institute of Atmospheric Sciences, Fudan University,  
7 Shanghai, 200438, China

8 *Correspondence to:* Tong Zhu (tzhu@pku.edu.cn)

9 **Abstract.** The reaction of SO<sub>2</sub> with NO<sub>2</sub> on the surface of aerosol particles has been suggested to be important in  
10 sulfate formation during severe air pollution episodes in China. However, we found that the direct oxidation of  
11 SO<sub>2</sub> by NO<sub>2</sub> was slow and might not be the main reason for sulfate formation in ambient air. In this study, we  
12 investigated the multiphase reaction of SO<sub>2</sub> with an O<sub>2</sub>/NO<sub>2</sub> mixture on single CaCO<sub>3</sub> particles using  
13 Micro-Raman spectroscopy. The reaction converted the CaCO<sub>3</sub> particle to a Ca(NO<sub>3</sub>)<sub>2</sub> droplet, with CaSO<sub>4</sub>•2H<sub>2</sub>O  
14 solid particles embedded in it, which constituted a significant fraction of the droplet volume at the end of the  
15 reaction. The reactive uptake coefficient of SO<sub>2</sub> for sulfate formation was on the order of 10<sup>-5</sup>, which was higher  
16 than that for the multiphase reaction of SO<sub>2</sub> directly with NO<sub>2</sub> by 2–3 orders of magnitude. According to our  
17 observations and the literature, we found that in the multiphase reaction of SO<sub>2</sub> with the O<sub>2</sub>/NO<sub>2</sub> mixture, O<sub>2</sub> was  
18 the main oxidant of SO<sub>2</sub> and was necessary for radical chain propagation. NO<sub>2</sub> acted as the initiator of radical  
19 formation, but not as the main oxidant. The synergy of NO<sub>2</sub> and O<sub>2</sub> resulted in much faster sulfate formation than  
20 the sum of the reaction rates with NO<sub>2</sub> and with O<sub>2</sub> alone. We estimated that the multiphase oxidation of SO<sub>2</sub> by  
21 O<sub>2</sub> initiated by NO<sub>2</sub> could be an important source of sulfate and a sink of SO<sub>2</sub>, based on the calculated lifetime of  
22 SO<sub>2</sub> regarding the loss through the multiphase reaction versus the loss through the gas-phase reaction with OH  
23 radical. Parameterizing the reactive uptake coefficient of the reaction observed in our laboratory for further model  
24 simulation is needed, as well as an integrated assessment based on field observations, laboratory study results,  
25 and model simulations to evaluate the importance of the reaction in ambient air during severe air pollution  
26 episodes, especially in China.

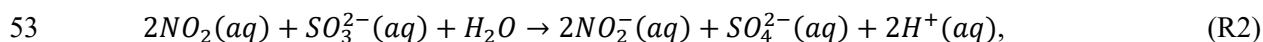
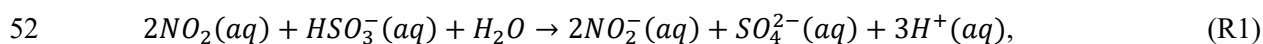
## 27 1 Introduction

28 It has been suggested that multiphase or heterogeneous oxidation of SO<sub>2</sub> potentially plays an important role  
29 in sulfate formation in the atmosphere (Seinfeld and Pandis, 2006). During the severe pollution episodes that  
30 occur frequently in China, high sulfate concentrations cannot be explained by the gas phase oxidation of SO<sub>2</sub> and  
31 its well-known aqueous chemistry (Zheng et al., 2015a; Cheng et al., 2016), highlighting the role of  
32 under-appreciated heterogeneous oxidation or multiphase pathways.

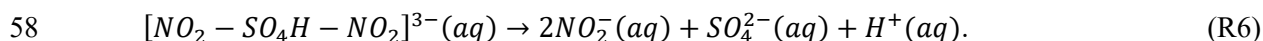
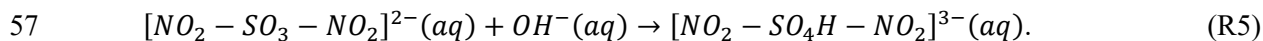
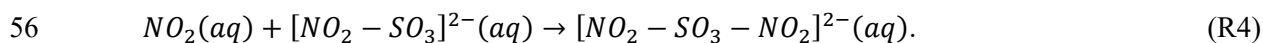
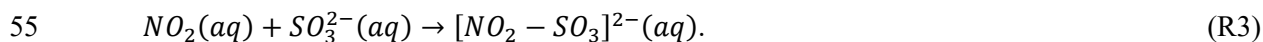
33 Recently, the multiphase oxidation of SO<sub>2</sub> by NO<sub>2</sub> has been introduced in air quality model simulations to  
34 explain the discrepancy between the modeled and observed sulfate concentration during severe pollution episodes  
35 in China (Cheng et al., 2016; Gao et al., 2016; Wang et al., 2016; Xue et al., 2016), despite the uncertainties in  
36 the kinetic parameters for SO<sub>2</sub> oxidation and in the pH value of aerosol particles in China (Wang et al., 2016;  
37 Cheng et al., 2016; Liu et al., 2017; Guo et al., 2017). However, according to our recently published results (Zhao  
38 et al., 2017), the direct oxidation of SO<sub>2</sub> by NO<sub>2</sub> could not contribute significantly to sulfate formation in the  
39 atmosphere because the reactive uptake coefficient of SO<sub>2</sub> for sulfate formation due to direct oxidation by NO<sub>2</sub> is  
40 very low ( $\sim 10^{-8}$ ).

41 Although the contribution of the direct oxidation of SO<sub>2</sub> by NO<sub>2</sub> to sulfate formation is not significant, NO<sub>2</sub>  
42 may be involved in other oxidation pathways of SO<sub>2</sub>. It has been reported that the reaction of NO<sub>2</sub> with SO<sub>3</sub><sup>2-</sup> and  
43 HSO<sub>3</sub><sup>-</sup> in the bulk aqueous phase can form the SO<sub>3</sub><sup>•-</sup> radical, which can further react with O<sub>2</sub> and produce a series  
44 of radicals that oxidize S(IV) species (Littlejohn et al., 1993). The reaction pathway may result in a fast SO<sub>2</sub>  
45 oxidation due to the potential synergy of NO<sub>2</sub> and O<sub>2</sub>.

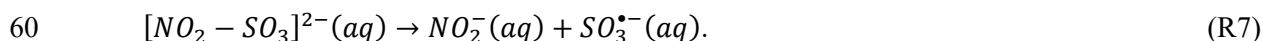
46 Despite such a reaction mechanism for SO<sub>2</sub> oxidation being proposed, its role in SO<sub>2</sub> oxidation in the  
47 ambient atmosphere is not well established. Most previous studies have focused on the direct reaction of SO<sub>2</sub>  
48 with NO<sub>2</sub>, including the determination of its rate constant (Lee and Schwartz, 1983; Clifton et al., 1988; Shen and  
49 Rochelle, 1998; Spindler et al., 2003; Nash, 1979; Huie and Neta, 1986). According to the reaction products and  
50 their reported yields (Lee and Schwartz, 1983; Clifton et al., 1988), the overall reaction equations of the direct  
51 reaction of SO<sub>2</sub> with NO<sub>2</sub> are as follows:



54 and the reactions are proposed to proceed via NO<sub>2</sub>-S(IV) adduct complexes (Clifton et al., 1988).



59 Additionally, NO<sub>2</sub>-S(IV) adduct complex may decompose as follows (Spindler et al., 2003).



61 However, studies of the oxidation rate of SO<sub>2</sub> at the O<sub>2</sub> concentrations relevant to the ambient atmosphere and the  
62 potential influence of the synergy of NO<sub>2</sub> and O<sub>2</sub> on the oxidation rate are very limited (Turšič et al., 2001; He et  
63 al., 2014), except a few studies investigated SO<sub>2</sub> oxidation in the presence of NO<sub>2</sub> as well as O<sub>2</sub> (Littlejohn et al.,  
64 1993; Shen and Rochelle, 1998; Santachiara et al., 1990). Moreover, previous studies have mainly focused on the

65 reaction in bulk solution and only few studies have investigated the oxidation of SO<sub>2</sub> by NO<sub>2</sub> on aerosol particles  
66 (Santachiara et al., 1990, 1993). On aerosol particles, water activity, pH, ionic strength, the presence of other  
67 compounds or ions, and the role of particle surface are different from in dilute bulk solution and may affect the  
68 reaction process and reaction rate. Therefore, further studies of the multiphase reaction of SO<sub>2</sub> with O<sub>2</sub>/NO<sub>2</sub>  
69 mixtures on aerosol particles are required to determine the kinetic parameters and the mechanism of the reaction.

70 In this study, we investigated the multiphase reaction of SO<sub>2</sub> with O<sub>2</sub> in the presence of NO<sub>2</sub> on CaCO<sub>3</sub>  
71 particles. We quantified the reactive uptake coefficient of SO<sub>2</sub> due to the reaction with an O<sub>2</sub>/NO<sub>2</sub>/H<sub>2</sub>O mixture.  
72 Based on our observations and the existing literature, we further discussed the reaction mechanism. Furthermore,  
73 we estimated the role of the multiphase oxidation of SO<sub>2</sub> by O<sub>2</sub> in the presence of NO<sub>2</sub> in the atmosphere.

## 74 2 Experimental

75 The experiments were conducted using a flow reaction system and the setup is shown in Fig. S1. The  
76 experimental setup and procedure used have been described in detail in previous studies (Zhao et al., 2017; Zhao  
77 et al., 2011; Liu et al., 2008). A gas mixture of NO<sub>2</sub>, SO<sub>2</sub>, O<sub>2</sub>, N<sub>2</sub>, and water vapor reacted with particles  
78 deposited on a substrate in the flow reaction cell. The concentrations of SO<sub>2</sub> and NO<sub>2</sub> were controlled using mass  
79 flow controllers by varying the flow rates of SO<sub>2</sub> (2,000 ppm in high purity N<sub>2</sub>, National Institute of Metrology  
80 P.R. China), NO<sub>2</sub> (1,000 ppm in high purity N<sub>2</sub>, Messer, Germany), and synthetic air [20% O<sub>2</sub> (high purity grade:  
81 99.999%, Beijing Haikeyuanchang Practical Gas Co., Ltd.) and 80% N<sub>2</sub> (high purity grade: 99.999%, Beijing  
82 Haikeyuanchang Practical Gas Co., Ltd.)]. Relative humidity (RH) was controlled by regulating the flow rates of  
83 reactant gases, dry synthetic air, and humidified synthetic air. Humidified synthetic air was prepared by bubbling  
84 synthetic air through fritted glass in water. In some experiments, the O<sub>2</sub> concentrations were varied by regulating  
85 the mixing ratios of O<sub>2</sub> and N<sub>2</sub> to investigate the effect of O<sub>2</sub>. SO<sub>2</sub>/O<sub>2</sub>/NO<sub>2</sub>/H<sub>2</sub>O mixtures flew through the  
86 reaction cell and reacted with individual stationary CaCO<sub>3</sub> particles, which were deposited on a Teflon-FEP film  
87 substrate annealed to a silicon wafer. RH and temperature were measured using a hygrometer (HMT100, Vaisala,  
88 Vantaa, Finland) at the exit of the reaction cell. Additionally, temperature was measured using another small  
89 temperature sensor (Pt 100, 1/3 DIN B, Heraeus, Hanau, Germany) in the reaction cell. All the experiments were  
90 conducted at 298 ± 0.5 K. The experiments were conducted under two RHs (72% and 82%) at 75 ppm SO<sub>2</sub> and  
91 75 ppm NO<sub>2</sub>.

92 During the reaction, particles were monitored *in-situ* via a glass window on the top of the reaction cell using  
93 a Micro-Raman spectrometer (LabRam HR800, HORIBA Jobin Yvon, Kyoto, Japan) to obtain microscopic  
94 images and Raman spectra. A 514-nm excitation laser was used, and back scattering Raman signals were detected.  
95 The details of the instrument are described elsewhere (Liu et al., 2008; Zhao et al., 2011). Because the particles  
96 were larger than the laser spot in this study (~1.5 μm), confocal Raman mapping was used to measure the spectra  
97 at different locations on a particle to obtain the chemical information of the entire particle. The mapping area was  
98 rectangular and was slightly larger than the particle, with mapping steps of 1 × 1 μm. Raman spectra in the range  
99 of 800–3,900 cm<sup>-1</sup> were acquired with an exposure time of 1 s for each mapping point. Raman spectra were  
100 analyzed using Labspec 5 software (HORIBA Jobin Yvon). Raman peaks were fitted to Gaussian–Lorentzian

101 functions to obtain peak positions and peak areas at different locations on the particle. The peak areas were then  
102 added together to obtain the peak area for the entire particle.

103 Particles of CaCO<sub>3</sub> (98%, Sigma-Aldrich, USA), with average diameters of about 7–10 μm as specified by  
104 the supplier, were used in the experiments. The CaCO<sub>3</sub> particles were rhombohedron crystals; X-ray diffraction  
105 analysis indicated that they were calcite (Fig. S2). Individual particles were prepared by dripping a dilute CaCO<sub>3</sub>  
106 suspended solution onto Teflon-FEP film using a pipette and then drying the sample in an oven at 80°C for 10 h.

107 The amount of CaSO<sub>4</sub> as a reaction product was quantified based on Raman peak areas and particle sizes.  
108 The details of the method are described in our previous study (Zhao et al., 2017). Briefly, the amount of reaction  
109 product CaSO<sub>4</sub> formed was determined as a function of time using Raman peak areas. Raman peak areas were  
110 converted to the amount of compound formed using a calibration curve obtained from pure CaSO<sub>4</sub> particles of  
111 different sizes, which were determined according to microscopic images. The reaction rate, i.e., the sulfate  
112 production rate, was derived from the amount of sulfate formed as a function of time. The reactive uptake  
113 coefficient of SO<sub>2</sub> for sulfate formation ( $\gamma$ ) was further determined from the reaction rate and collision rate of SO<sub>2</sub>  
114 on the surface of a single particle.

$$115 \quad \gamma = \frac{d\{SO_4^{2-}\}}{Z} \cdot \quad (1)$$

$$116 \quad Z = \frac{1}{4}cA_s[SO_2], \quad (2)$$

$$117 \quad c = \sqrt{\frac{8RT}{\pi M_{SO_2}}}, \quad (3)$$

118 where R is the gas constant, T is temperature, M<sub>SO<sub>2</sub></sub> is the molecular weight of SO<sub>2</sub>, c is the mean molecular  
119 velocity of SO<sub>2</sub>, A<sub>s</sub> is the surface area of an individual particle, and Z is the collision rate of SO<sub>2</sub> on the surface of  
120 a particle. {SO<sub>4</sub><sup>2-</sup>} indicates the amount of sulfate in the particle phase in moles. The average reaction rate and  
121 surface area of particles during the multiphase reaction period were used to derive the reactive uptake coefficient.  
122 The period was chosen to start after the induction period when ~10% of the final sulfate was formed. [SO<sub>2</sub>]  
123 indicates the concentration of SO<sub>2</sub> in the gas phase.

124 The influence of gas phase diffusion on reactive uptake was evaluated using the resistor model described by  
125 Davidovits et al. (2006) and references therein, as well as using the gas phase diffusion correction factor for a  
126 reactive uptake coefficient according to the method described by Pöschl et al. (2007). The reactive uptake of SO<sub>2</sub>  
127 was found to not be limited by gas phase diffusion (see details in the Supplement S1).

128 In addition, we conducted experiments of the reaction SO<sub>2</sub> with only O<sub>2</sub> on both CaCO<sub>3</sub> solid particles and  
129 internally mixed CaCO<sub>3</sub>/Ca(NO<sub>3</sub>)<sub>2</sub> particles (with CaCO<sub>3</sub> embedded in Ca(NO<sub>3</sub>)<sub>2</sub> droplets), while keeping other  
130 conditions the same as the reaction of SO<sub>2</sub> with an O<sub>2</sub>/NO<sub>2</sub> mixture. These experiments of the multiphase  
131 oxidation of SO<sub>2</sub> by O<sub>2</sub> can help determine the role of NO<sub>2</sub> in the reaction of SO<sub>2</sub> with an O<sub>2</sub>/NO<sub>2</sub> mixture.

## 132 3 Results and discussion

### 133 3.1 Reaction products and changes in particle morphology

134 Figure 1 shows the Raman spectra of a CaCO<sub>3</sub> particle during the multiphase reaction of SO<sub>2</sub> with O<sub>2</sub>/NO<sub>2</sub>/H<sub>2</sub>O  
135 on its surface. The peak at 1,087 cm<sup>-1</sup> was assigned to the symmetric stretching of carbonate ( $\nu_s(\text{CO}_3^{2-})$ )

136 (Nakamoto, 1997). During the reaction, the peak at  $1,087\text{ cm}^{-1}$  decreased continuously and finally disappeared as  
137 new peaks were observed. The peak at  $1,050\text{ cm}^{-1}$  was assigned to the symmetric stretching of nitrate ( $\nu_s(\text{NO}_3^-)$ ).  
138 The peaks at  $1,010\text{ cm}^{-1}$  and  $1,136\text{ cm}^{-1}$  were assigned to the symmetric stretching ( $\nu_s(\text{SO}_4^{2-})$ ) and asymmetric  
139 stretching ( $\nu_{as}(\text{SO}_4^{2-})$ ) of sulfate in gypsum ( $\text{CaSO}_4 \cdot 2\text{H}_2\text{O}$ ), respectively (Sarma et al., 1998). In addition, after the  
140 reaction, a broad envelope in the range of  $2,800\text{--}3,800\text{ cm}^{-1}$  assigned to the stretching of the OH bond in water  
141 molecules was observed. Above this envelope, there were two peaks at  $3,408\text{ cm}^{-1}$  and  $3,497\text{ cm}^{-1}$ , which were  
142 assigned to OH bond stretching in crystallization water of  $\text{CaSO}_4 \cdot 2\text{H}_2\text{O}$  (Sarma et al., 1998; Ma et al., 2013).

143 During the multiphase reaction with the  $\text{SO}_2/\text{O}_2/\text{NO}_2/\text{H}_2\text{O}$  mixture, the  $\text{CaCO}_3$  particles displayed a remarkable  
144 change in morphology. The original  $\text{CaCO}_3$  particle was a rhombohedron crystal (Fig. 2, panel i, a). As the  
145 reaction proceeded, its edges became smoother and later a transparent droplet layer formed, which had a newly  
146 formed solid phase embed in it (Fig. 2, panel i, d). The size of the new solid phase grew during the reaction (Fig.  
147 2, panel i, d–f) and it seemed to contain many micro-crystals. Raman mapping revealed that the new solid phase  
148 consisted of  $\text{CaSO}_4 \cdot 2\text{H}_2\text{O}$  (Fig. 2, panel iv), and the surrounding aqueous layer consisted of  $\text{Ca}(\text{NO}_3)_2$  (Fig. 2,  
149 panel iii).

150 The particle morphology change shown in Fig. 2 was significantly different from the morphology change in  
151 the direct reaction of  $\text{SO}_2$  with  $\text{NO}_2$  (Zhao et al., 2017), where the  $\text{CaCO}_3$  particle was first converted to a  
152 spherical  $\text{Ca}(\text{NO}_3)_2$  droplet and then needle-shaped  $\text{CaSO}_4$  crystals formed inside the droplet (Zhao et al., 2017).  
153 Moreover, the amount of  $\text{CaSO}_4$  formed in this study was much higher than that in the direct reaction of  $\text{SO}_2$  with  
154  $\text{NO}_2$ . The  $\text{CaSO}_4$  solid particle constituted a significant fraction of the volume of the droplet, while in the direct  
155 reaction of  $\text{SO}_2$  with  $\text{NO}_2$  the few needle-shaped  $\text{CaSO}_4$  crystals that formed only constituted a small fraction of  
156 the droplet volume (Zhao et al., 2017).

### 157 3.2 Reaction process

158 During the reaction, the amounts of carbonate, nitrate, and sulfate were determined as a function of time, as  
159 shown in Fig. 3. At the beginning of the reaction, the amount of carbonate decreased slowly, while the amount of  
160 nitrate and sulfate increased slowly. After a period of induction of around 50 min, the reaction accelerated  
161 significantly, leading to a rapid consumption of carbonate and production of nitrate and sulfate. The decrease in  
162 the amount of carbonate and the increase in the amount of nitrate was because carbonate reacted continuously  
163 with  $\text{NO}_2$  and  $\text{H}_2\text{O}$ , forming  $\text{Ca}(\text{NO}_3)_2$ . The detailed mechanism of the multiphase reaction of carbonate with  $\text{NO}_2$   
164 and  $\text{H}_2\text{O}$  were discussed in our previous studies (Li et al., 2010; Zhao et al., 2017). The mechanism of sulfate  
165 formation is discussed in detail in Section 3.4 of the present study. Finally, the carbonate was completely  
166 consumed, and the amounts of nitrate and sulfate levelled off.

167 Figure 3 shows that nitrate and sulfate were formed simultaneously during the reaction. This contrasts with  
168 the observations made during the direct reaction of  $\text{SO}_2$  with  $\text{NO}_2$ , where nitrate was formed first, and sulfate was  
169 essentially formed after the complete conversion of  $\text{CaCO}_3$  particles to  $\text{Ca}(\text{NO}_3)_2$  droplets (Zhao et al., 2017).  
170 Moreover, the time taken for carbonate to be completely consumed was longer in this study than in the direct  
171 reaction of  $\text{SO}_2$  with  $\text{NO}_2$  ( $\sim 120$  vs.  $\sim 40$  min) when other conditions were kept the same (Zhao et al., 2017).

### 172 3.3 Reactive uptake coefficient of SO<sub>2</sub>

173 The reactive uptake coefficients of SO<sub>2</sub> for sulfate formation ( $\gamma$ ) in the reaction of SO<sub>2</sub> with the  
174 O<sub>2</sub>/NO<sub>2</sub>/H<sub>2</sub>O/N<sub>2</sub> mixture on CaCO<sub>3</sub> with various O<sub>2</sub> concentrations are shown in Table 1. The value of  $\gamma$  for the  
175 reaction of SO<sub>2</sub> with O<sub>2</sub>/NO<sub>2</sub> at three O<sub>2</sub> concentrations (5, 20, and 86%) was in the range of  $(0.35\text{--}1.7) \times 10^{-5}$ ,  
176 and was  $1.2 \times 10^{-5}$  in synthetic air. This latter value was 2–3 orders of magnitude higher than that for the reaction  
177 of SO<sub>2</sub> directly with NO<sub>2</sub> under similar conditions (Zhao et al., 2017). When other conditions were kept constant,  
178  $\gamma$  increased with the O<sub>2</sub> concentration. This indicates that O<sub>2</sub> played a key role in enhancing the oxidation rate of  
179 SO<sub>2</sub>.

180 The role of O<sub>2</sub> in enhancing the reactive uptake of SO<sub>2</sub> reported here is consistent with the findings in some  
181 previous studies. For example, Littlejohn et al. (1993)'s data showed that sulfite oxidation rate increases with the  
182 O<sub>2</sub> concentration (0–5% by volume). Shen and Rochelle (1998) also found that in the presence of O<sub>2</sub>, the aqueous  
183 sulfite oxidation rate is enhanced. By investigating the oxidation of SO<sub>2</sub> by NO<sub>2</sub> in monodispersed water droplets  
184 growing on carbon nuclei, Santachiara et al. (1990) found that sulfate formation rate with 2% O<sub>2</sub> is much higher  
185 than that without O<sub>2</sub>. Yet, our findings, as well as those in the studies referred to above, are in contrast to those  
186 reported by Lee and Schwartz (1983), who found that changing from N<sub>2</sub> to air as a carrier gas only increases  
187 bisulfite oxidation rate by no more than 10%. The difference between our study and Lee and Schwartz (1983)  
188 could be due to the difference in O<sub>2</sub> diffusion from gas to the condensed phase and the different mechanisms  
189 between the multiphase reaction on particles and the aqueous reaction.

190 Only few studies have reported the S(IV) oxidation rate in the reaction of S(IV) with O<sub>2</sub>/NO<sub>2</sub> mixtures  
191 (Turšič et al., 2001; Littlejohn et al., 1993). However, due to the limiting step by the aqueous phase mass transfer,  
192 it is difficult to quantitatively compare the reaction rates in those studies with the uptake coefficient in our study  
193 and the rate constants determined by Lee and Schwartz (1983) and Clifton et al. (1988). For example, a rate  
194 constant of  $2.4 \times 10^3 \text{ mol}^{-1} \text{ L s}^{-1}$  (at pH 3) can be derived from the results of Turšič et al. (2001), which is much  
195 lower than the values reported by Lee and Schwartz (1983) and Clifton et al. (1988). This can be attributed to the  
196 limiting step by the aqueous-phase mass transfer because the characteristic mixing time in the aqueous phase in  
197 Turšič et al. (2001) was likely much longer than that of Lee and Schwartz (1983) (1.7–5.3 s), according to the  
198 HSO<sub>3</sub><sup>-</sup> concentration time series reported by Turšič et al. (2001).

199 It is important to note that the concentrations of NO<sub>2</sub> and SO<sub>2</sub> used in this study are much higher than those  
200 in the ambient atmosphere. High concentrations of reactant gases are often used in laboratory studies in order to  
201 simulate the ambient reactions at the time scale of days or weeks and to get high signal-to-noise ratios for  
202 detecting products within minutes or hours. In the ambient atmosphere, reactive uptake coefficient of SO<sub>2</sub> should  
203 be lower than that in this study due to the lower NO<sub>2</sub> concentrations when other conditions are comparable and  
204 the chemical/physical processes observed in this study, such as changes in particle composition, phase,  
205 hygroscopicity, and pH should be much slower due to the lower concentrations of NO<sub>2</sub> and SO<sub>2</sub>.

### 206 3.4 Reaction mechanism

207 In the multiphase reaction of SO<sub>2</sub> with O<sub>2</sub>/NO<sub>2</sub>/H<sub>2</sub>O on CaCO<sub>3</sub> particles, we found that CaCO<sub>3</sub> reacted with  
208 NO<sub>2</sub> and H<sub>2</sub>O and produced Ca(NO<sub>3</sub>)<sub>2</sub>, which deliquesced, forming liquid water, and provided a site for the

209 aqueous oxidation of SO<sub>2</sub>. This process is similar to the direct reaction of SO<sub>2</sub> with NO<sub>2</sub> on CaCO<sub>3</sub> particles. The  
210 details of this part of the reaction mechanism were discussed in our previous study (Zhao et al., 2017).

211 Once the aqueous phase was formed, SO<sub>2</sub> could undergo multiphase reactions with O<sub>2</sub>/NO<sub>2</sub>. The mechanism  
212 of the direct aqueous reaction of S(IV) with NO<sub>2</sub> in the absence of O<sub>2</sub> is complex. Previous studies have proposed  
213 two different mechanisms for the reaction. One involves SO<sub>3</sub><sup>•-</sup> radical formation (Littlejohn et al., 1993; Shen and  
214 Rochelle, 1998; Turšič et al., 2001) (referred as “free-radical chain” mechanism, while the other involves the  
215 formation of NO<sub>2</sub>-S(IV) complexes (Clifton et al., 1988), but no radical formation (referred as “NO<sub>2</sub>-S(IV)  
216 complex” mechanism).

217 According to the NO<sub>2</sub>-S(IV) complex mechanism, the presence of O<sub>2</sub> should not affect the SO<sub>2</sub> oxidation  
218 rate; however, in this study, a substantial enhancement in the SO<sub>2</sub> oxidation rate was observed in the presence of  
219 O<sub>2</sub> compared with that in the absence of O<sub>2</sub>. Therefore, the NO<sub>2</sub>-S(IV) complex mechanism was less likely to  
220 have been important in this study.

221 In the free-radical chain mechanism, the SO<sub>3</sub><sup>•-</sup> radical is proposed to be formed (R8, Table 2), which is based  
222 on the observation of S<sub>2</sub>O<sub>6</sub><sup>2-</sup> formation, with S<sub>2</sub>O<sub>6</sub><sup>2-</sup> known to be the combination reaction product of SO<sub>3</sub><sup>•-</sup>  
223 (Eriksen, 1974; Hayon et al., 1972; Deister and Warneck, 1990; Brandt et al., 1994; Waygood and McElroy,  
224 1992). In addition to SO<sub>4</sub><sup>2-</sup> and NO<sub>2</sub><sup>-</sup>, S<sub>2</sub>O<sub>6</sub><sup>2-</sup> was detected with an appreciable yield using Raman spectroscopy,  
225 following the reaction of NO<sub>2</sub> with aqueous sulfite (Littlejohn et al., 1993). S<sub>2</sub>O<sub>6</sub><sup>2-</sup> was also observed in the  
226 aqueous oxidation of bisulfite in an N<sub>2</sub>-saturated solution in the presence of Fe(III) using ion-interaction  
227 chromatography (Podkrajšek et al., 2002). The SO<sub>3</sub><sup>•-</sup> radical can react via two pathways, forming either S<sub>2</sub>O<sub>6</sub><sup>2-</sup> or  
228 SO<sub>4</sub><sup>2-</sup> (R9–R11, Table 2). The reactions R9–R11 have been well established in studies of S(IV) oxidation by  
229 other pathways, including OH oxidation, photo-oxidation, and transition metal catalyzed oxidation (Eriksen, 1974;  
230 Hayon et al., 1972; Deister and Warneck, 1990; Brandt et al., 1994; Brandt and Vaneldik, 1995; Waygood and  
231 McElroy, 1992). In addition, although previous studies have not reported the direct observation of the SO<sub>3</sub><sup>•-</sup>  
232 radical in the aqueous reaction of S(IV) with NO<sub>2</sub>, SO<sub>3</sub><sup>•-</sup> was observed in the reaction of NO<sub>2</sub><sup>-</sup> with SO<sub>3</sub><sup>2-</sup> in an  
233 acidic buffer solution (pH = 4.0) using electron spin resonance (ESR) (Shi, 1994). Because NO<sub>2</sub><sup>-</sup> is formed in the  
234 aqueous reaction of SO<sub>2</sub> with NO<sub>2</sub>, and S<sub>2</sub>O<sub>6</sub><sup>2-</sup> as the combination reaction product of SO<sub>3</sub><sup>•-</sup> is observed (Littlejohn  
235 et al., 1993), SO<sub>3</sub><sup>•-</sup> formation is plausible.

236 In the presence of O<sub>2</sub>, the SO<sub>3</sub><sup>•-</sup> radical can react rapidly with O<sub>2</sub>, forming the SO<sub>5</sub><sup>•-</sup> radical (R12, Table 2).  
237 Following this reaction, a number of chain reactions can occur to ultimately form sulfate (Littlejohn et al., 1993;  
238 Seinfeld and Pandis, 2006; Shen and Rochelle, 1998) (R13–R16, Table 2). Littlejohn et al. (1993) observed that  
239 the amount of S<sub>2</sub>O<sub>6</sub><sup>2-</sup> relative to SO<sub>4</sub><sup>2-</sup> formed in the aqueous reaction of NO<sub>2</sub> with sulfite decreases in the  
240 presence of O<sub>2</sub> compared with the reaction in the absence of O<sub>2</sub>. At low NO<sub>2</sub> concentrations (< 5 ppm), S<sub>2</sub>O<sub>6</sub><sup>2-</sup> is  
241 undetectable in the presence of O<sub>2</sub>. This indicates that O<sub>2</sub> suppresses the reaction pathway of S<sub>2</sub>O<sub>6</sub><sup>2-</sup> formation  
242 (R9, Table 2). Because the SO<sub>3</sub><sup>•-</sup> radical can react rapidly with O<sub>2</sub>, forming the SO<sub>5</sub><sup>•-</sup> radical, and would therefore  
243 be consumed, the suppression of S<sub>2</sub>O<sub>6</sub><sup>2-</sup> formation can be attributed to the reaction of SO<sub>3</sub><sup>•-</sup> with O<sub>2</sub> (R12, Table  
244 2). The reactions R12–R16 have been well established by studies of the oxidation of S(IV) by OH or  
245 photo-oxidation, and all the radicals have been observed (Hayon et al., 1972; Huie et al., 1989; Huie and Neta,  
246 1987; Chameides and Davis, 1982; Seinfeld and Pandis, 2006).

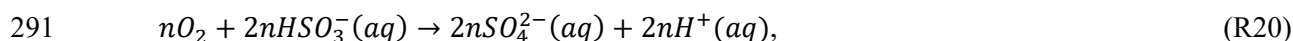
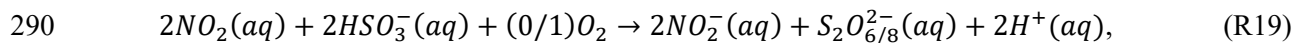
247 The free-radical chain mechanism is consistent with the findings of this study and is therefore more plausible.  
248 The enhancement of the SO<sub>2</sub> oxidation rate in the reaction of SO<sub>2</sub> with O<sub>2</sub>/NO<sub>2</sub>/H<sub>2</sub>O on CaCO<sub>3</sub> particles  
249 compared with that in the direct reaction of SO<sub>2</sub> with NO<sub>2</sub>/H<sub>2</sub>O was attributed to O<sub>2</sub>. Although during the reaction  
250 in the absence of O<sub>2</sub>—i.e., the direct oxidation of SO<sub>2</sub> by NO<sub>2</sub>—the SO<sub>3</sub><sup>•-</sup> radical can be formed (R7), the reaction  
251 chain cannot propagate (R12–R16). Therefore, the S(IV) oxidation rate and the reactive uptake coefficient of SO<sub>2</sub>  
252 were much lower than that in the presence of O<sub>2</sub>. According to the difference between the reactive uptake  
253 coefficient in this study and in the direct reaction of SO<sub>2</sub> with NO<sub>2</sub> (Zhao et al., 2017), the sulfate production rate  
254 via chain reactions due to the presence of O<sub>2</sub> (20%) was 2–3 orders of magnitude faster than the direct oxidation  
255 of SO<sub>2</sub> by NO<sub>2</sub>. This indicates that sulfate production in the reaction of SO<sub>2</sub> with O<sub>2</sub>/NO<sub>2</sub> was largely due to O<sub>2</sub>  
256 oxidation via the chain reaction pathway, i.e., “autoxidation” of S(IV), rather than the direct oxidation of SO<sub>2</sub> by  
257 NO<sub>2</sub> and thus O<sub>2</sub> was the main oxidant of SO<sub>2</sub>.

258 In addition to the two mechanisms above, Spindler et al. (2003) proposed a reaction mechanism involving  
259 first NO<sub>2</sub>–S(IV) complex formation and subsequent SO<sub>3</sub><sup>•-</sup> radical formation (R3, R7). NO<sub>2</sub>–S(IV) complex may  
260 establish an equilibrium with SO<sub>3</sub><sup>•-</sup> in contrast to the direct formation of SO<sub>3</sub><sup>•-</sup> via the reaction of NO<sub>2</sub> with SO<sub>2</sub>.  
261 Higher concentration of O<sub>2</sub> favors the conversion of SO<sub>3</sub><sup>•-</sup> to SO<sub>5</sub><sup>•-</sup> and thus can reduce the SO<sub>3</sub><sup>•-</sup> concentration,  
262 shifting the equilibrium to the product side and promoting the overall S(IV) oxidation. O<sub>2</sub> can act in a similar way  
263 as in the free-radical chain mechanism. Admittedly, we cannot rule out the possibility NO<sub>2</sub>–S(IV) complex  
264 formation. But such a mechanism can still be classified as the free-radical chain mechanism since the S(IV)  
265 oxidation still proceeds via the radical chain reactions. Although the direct oxidation of SO<sub>2</sub> by NO<sub>2</sub> only  
266 accounted for a very small fraction of sulfate formation, NO<sub>2</sub> played an important role in the SO<sub>2</sub> oxidation by  
267 initiating the chain reactions via the production of the SO<sub>3</sub><sup>•-</sup> radical (R7). In the experiment without NO<sub>2</sub>, but with  
268 other reaction conditions the same, we were unable to detect sulfate after 5 h of reaction. This indicates that O<sub>2</sub> by  
269 itself cannot initiate the chain reactions (although it favors chain propagation), and that the oxidation of SO<sub>2</sub> by  
270 O<sub>2</sub> was slow. The effect on the SO<sub>2</sub> oxidation rate when both NO<sub>2</sub> and O<sub>2</sub> were present was much higher than the  
271 sum of the effect of NO<sub>2</sub> and O<sub>2</sub>. We refer to this effect as the synergy of NO<sub>2</sub> and O<sub>2</sub>, which resulted in the fast  
272 oxidation of SO<sub>2</sub> to form sulfate in this study. This effect is similar to a “ternary” reaction found with the reaction  
273 of NO<sub>2</sub>–particles–H<sub>2</sub>O or SO<sub>2</sub>–particles–O<sub>3</sub> (Zhu et al., 2011), where the reaction rate can be much faster than the  
274 sum of the reaction rates for the reaction of the second and third reactant with the first reactant. In addition to  
275 acting as the initiator of chain reactions, NO<sub>2</sub> also contributed to the formation of the aqueous phase through the  
276 reaction with CaCO<sub>3</sub>, forming Ca(NO<sub>3</sub>)<sub>2</sub> as discussed above, which provided a site for S(IV) oxidation.

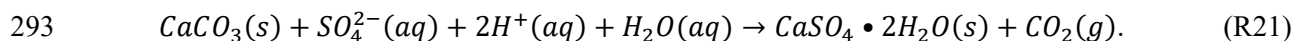
277 Based on the discussion above, we summarize the reaction mechanism that occurred in this study in Table 2.  
278 The reactions are classified as chain initiation, chain propagation, and chain termination. The dominant S(IV)  
279 species depends on pH. Due to the fast dissociations of SO<sub>2</sub>•H<sub>2</sub>O and HSO<sub>3</sub><sup>-</sup>, reactions consuming one of these  
280 S(IV) species will result in instantaneous re-establishment of the equilibria between them (Seinfeld and Pandis,  
281 2006). In this study, the pH of the aqueous layer of Ca(NO<sub>3</sub>)<sub>2</sub> may change dynamically with time during the  
282 reaction and may not be completely homogeneous within the aqueous droplet. The pH values could vary between  
283 ~3 and ~7.6. In the surface of the aqueous layer, pH was mainly determined by the gas–aqueous equilibrium of  
284 SO<sub>2</sub>, and was estimated to be ~3. In the vicinity of the CaCO<sub>3</sub> core, pH was mainly determined by the hydrolysis  
285 of carbonate and was estimated to be ~7.6. It is likely that both HSO<sub>3</sub><sup>-</sup> and SO<sub>3</sub><sup>2-</sup> were present, and the dominant



286 species depended on the reaction time and location within the aqueous droplet. Nevertheless, to make the reaction  
 287 mechanism clearer,  $\text{HSO}_3^-$  was used in the reaction equations. Similar reaction equations are also applicable to  
 288  $\text{SO}_3^{2-}$  because of the fast dissociations of  $\text{SO}_2 \cdot \text{H}_2\text{O}$  and  $\text{HSO}_3^-$ . Overall, the reaction can be written as follows,  
 289 which clearly shows that  $\text{O}_2$  was the main oxidant for sulfate formation:



292 where  $n \gg 1$ . Once sulfuric acid was formed, it reacted with  $\text{CaCO}_3$ , forming  $\text{CaSO}_4$ :



294 As mentioned above, compared with the direct reaction of  $\text{SO}_2$  with  $\text{NO}_2$ ,  $\text{CaCO}_3$  was consumed more  
 295 slowly in the reaction with  $\text{O}_2/\text{NO}_2$ . There were two possible reasons for this. First, the  $\text{CaSO}_4 \cdot 2\text{H}_2\text{O}$  formed in  
 296 the reaction could cover the  $\text{CaCO}_3$  surface and partly suppress the diffusion of aqueous ions, such as protons,  
 297 and also limit the contact of reactants with the surface of the  $\text{CaCO}_3$  particles, thus reducing the  $\text{CaCO}_3$   
 298 consumption rate. Second, compared with the direct reaction of  $\text{SO}_2$  with  $\text{NO}_2$ , a much higher fraction of  $\text{CaCO}_3$   
 299 was converted to  $\text{CaSO}_4 \cdot 2\text{H}_2\text{O}$  instead of  $\text{Ca}(\text{NO}_3)_2$  due to the fast production of  $\text{CaSO}_4 \cdot 2\text{H}_2\text{O}$ . Therefore, the  
 300 volume of a  $\text{Ca}(\text{NO}_3)_2$  droplet was much smaller than that in the direct reaction of  $\text{SO}_2$  with  $\text{NO}_2$  for a given  
 301  $\text{CaCO}_3$  particle. Because the uptake rate of  $\text{NO}_2$  was proportional to the droplet surface area and the  $\text{NO}_2$   
 302 hydrolysis rate was proportional to the droplet volume, the rate of nitric acid production from  $\text{NO}_2$  hydrolysis and  
 303 its reaction rate with  $\text{CaCO}_3$  were reduced. Therefore, the  $\text{CaCO}_3$  particles were consumed more slowly in the  
 304 reaction with  $\text{O}_2/\text{NO}_2$ .

#### 305 4 Conclusion and implications

306 We investigated the multiphase reaction of  $\text{SO}_2$  with  $\text{O}_2/\text{NO}_2/\text{H}_2\text{O}$  on  $\text{CaCO}_3$  particles. The reaction  
 307 converted  $\text{CaCO}_3$  particles to  $\text{Ca}(\text{NO}_3)_2$  droplets, in which  $\text{CaSO}_4 \cdot 2\text{H}_2\text{O}$  was embedded and accounted for a  
 308 significant fraction of the droplet volume by the end of the reaction. The  $\text{Ca}(\text{NO}_3)_2$  droplet formed by the reaction  
 309 of  $\text{CaCO}_3$  with  $\text{NO}_2$  provided a site for the multiphase oxidation of  $\text{SO}_2$ . Generally, nitrate and sulfate were  
 310 formed simultaneously. The reactive uptake coefficient of  $\text{SO}_2$  for sulfate formation in the reaction of  $\text{SO}_2$  with  
 311  $\text{NO}_2/\text{H}_2\text{O}$  in synthetic air was determined to be around  $10^{-5}$ . Compared with the reaction of  $\text{SO}_2$  with  $\text{NO}_2$  on a  
 312  $\text{CaCO}_3$  particle in the absence of  $\text{O}_2$ , i.e., the direct oxidation of  $\text{SO}_2$  by  $\text{NO}_2$  in  $\text{N}_2$ , sulfate production rate in the  
 313 reaction of  $\text{SO}_2$  with  $\text{O}_2/\text{NO}_2$  was enhanced by 2–3 orders of magnitude. According to the findings of this study  
 314 and the existing literature,  $\text{SO}_2$  oxidation likely proceeded via a free-radical chain reaction mechanism.  $\text{O}_2$  was  
 315 the main oxidant of  $\text{SO}_2$ , and  $\text{NO}_2$  mainly acted as an initiator of the chain reactions. The synergy of  $\text{NO}_2$  and  $\text{O}_2$   
 316 resulted in the fast oxidation of  $\text{SO}_2$ . The absence of either  $\text{NO}_2$  or  $\text{O}_2$  led to much slower  $\text{SO}_2$  oxidation.

317 Using a method developed in our previous study (Zhao et al., 2017), we assessed the importance of the  
 318 multiphase oxidation of  $\text{SO}_2$  by  $\text{O}_2$  in the presence of  $\text{NO}_2$  by estimating the lifetime of  $\text{SO}_2$  due to multiphase  
 319 reactions and the lifetime due to the gas phase reaction (with the OH radical). The lifetime of  $\text{SO}_2$  due to the  
 320 multiphase reaction of  $\text{SO}_2$  with  $\text{O}_2/\text{NO}_2$  was estimated to be around 20 days using the reactive uptake coefficient  
 321 of  $\text{SO}_2$  ( $1.2 \times 10^{-5}$ ) and the typical particle surface area concentration for mineral aerosols in winter in Beijing  
 322 ( $6.3 \times 10^{-6} \text{ cm}^2 \text{ cm}^{-3}$ ) (Huang et al., 2015). This lifetime is comparable to the lifetime of  $\text{SO}_2$  due to the gas phase

323 reaction with OH, which is ~12 days assuming that the daytime OH concentration is  $1 \times 10^6$  molecules  $\text{cm}^{-3}$   
324 (Lelieveld et al., 2016; Prinn et al., 2005). Therefore, we conclude that the multiphase oxidation of  $\text{SO}_2$  by  $\text{O}_2$  in  
325 the presence of  $\text{NO}_2$  is likely to be an important source of sulfate and a sink of  $\text{SO}_2$  in the ambient atmosphere,  
326 and can play a significant role in the sulfate formation during severe haze episodes, such as those that frequently  
327 occur in China. During haze episodes, there are high concentrations of  $\text{SO}_2$  and  $\text{NO}_2$  and relative humidity is  
328 often high (Zhang et al., 2014; Wang et al., 2016; Zheng et al., 2015b). Under these conditions, the multiphase  
329 oxidation of  $\text{SO}_2$  by  $\text{O}_2$  in the presence of  $\text{NO}_2$  could proceed rapidly, forming sulfate. The enhanced sulfate  
330 concentration due to multiphase reactions and resulting aerosol water content can further promote the multiphase  
331 oxidation of  $\text{SO}_2$ . The reaction thus proceeds in a self-accelerating way. Therefore, it can contribute significantly  
332 to sulfate formation during haze episodes, which could explain the discrepancies between the observed and  
333 modelled sulfate concentrations (Cheng et al., 2016; Gao et al., 2016; Wang et al., 2016; Zheng et al., 2015a).

334 In addition, elucidating the mechanism of the multiphase reaction of  $\text{SO}_2$  with  $\text{O}_2/\text{NO}_2/\text{H}_2\text{O}$  in the  
335 atmosphere is important for the other atmospheric implications of the reaction besides sulfate formation.  
336 According to the reaction mechanism, the direct oxidation of  $\text{SO}_2$  by  $\text{NO}_2$  forms sulfate and nitrite, with a  
337 stoichiometry of 1:1, and nitrite can further form HONO under acidic conditions. The HONO could then  
338 evaporate into the atmosphere, where it would be an important source of OH radical. If  $\text{NO}_2$  were the main  
339 oxidant of  $\text{SO}_2$  in the multiphase reaction, the reaction would form one HONO molecule for every sulfate formed.  
340 Thus, the oxidation of  $\text{SO}_2$  by  $\text{NO}_2$  can simultaneously be an important source of HONO and OH radical, and  
341  $\text{SO}_2$  oxidation would be strongly coupled with reactive nitrogen chemistry. However, according to the  
342 mechanism of this study,  $\text{NO}_2$  only acted as an initiator of the chain reactions in  $\text{SO}_2$  oxidation and essentially all  
343 the  $\text{SO}_2$  was oxidized by  $\text{O}_2$ . Therefore, the amount of HONO formation per sulfate formed was trivial. The  
344 oxidation of  $\text{SO}_2$  by  $\text{O}_2/\text{NO}_2$  is expected to be neither an important source of HONO and OH in the atmosphere  
345 nor to have a significant influence on reactive nitrogen chemistry.

346 In this study, we investigated the reaction of  $\text{SO}_2$  with  $\text{O}_2$  in the presence of  $\text{NO}_2$  at three  $\text{O}_2$  concentrations.  
347 The influence of the  $\text{O}_2$  concentration was shown to be significant. Future experimental results with more  $\text{O}_2$   
348 concentration levels would provide more insights into the reaction mechanism and process.

349 In addition, in the ambient atmosphere, the internal mixing of organics with S(IV) in particles may influence  
350 the S(IV) oxidation rate by  $\text{O}_2$  in the presence of  $\text{NO}_2$ . When organics is abundant in particles, for example during  
351 haze episodes in China, it can react with and thus scavenge radical anion carriers such as  $\text{SO}_5^{\cdot-}$  and  $\text{SO}_4^{\cdot-}$   
352 (Herrmann, 2003; Herrmann et al., 2015; Huie, 1995). Therefore, the presence of internally mixed organics can  
353 reduce the effectivity of the potential radical reaction chain and of S(IV) oxidation, which can undermine the  
354 importance of the oxidation by  $\text{O}_2$  in the presence of  $\text{NO}_2$  in the overall S(IV) oxidation.

### 355 **Acknowledgements**

356 This work was supported by Natural Science Foundation Committee of China (41421064, 21190051,  
357 40490265, 91544000) and Ministry of Science and Technology (Grant No. 2002CB410802).

358 **References**

- 359 Brandt, C., Fabian, I., and Vaneldik, R.: Kinetics and mechanism of the iron(III)-catalyzed autoxidation of  
360 sulfur(IV) oxides in aqueous-solution - evidence for the redox cycling of iron in the presence of oxygen and  
361 modeling of the overall reaction-mechanism, *Inorg. Chem.*, 33, 687-701, 10.1021/ic00082a012, 1994.
- 362 Brandt, C., and Vaneldik, R.: Transition metal-catalyzed oxidation of sulfur (IV) oxides. Atmospheric-relevant  
363 processes and mechanisms, *Chem. Rev.*, 95, 119-190, 10.1021/cr00033a006, 1995.
- 364 Chameides, W. L., and Davis, D. D.: The free-radical chemistry of cloud droplets and its impact upon the  
365 composition of rain, *J. Geophys. Res.-Oceans*, 87, 4863-4877, 10.1029/JC087iC07p04863, 1982.
- 366 Cheng, Y. F., Zheng, G. J., Wei, C., Mu, Q., Zheng, B., Wang, Z. B., Gao, M., Zhang, Q., He, K. B., Carmichael,  
367 G., Poschl, U., and Su, H.: Reactive nitrogen chemistry in aerosol water as a source of sulfate during haze events  
368 in China, *Sci. Adv.*, 2, 10.1126/sciadv.1601530, 2016.
- 369 Clifton, C. L., Altstein, N., and Huie, R. E.: Rate-constant for the reaction of NO<sub>2</sub> with sulfur(IV) over the pH  
370 range 5.3-13, *Environ. Sci. Technol.*, 22, 586-589, 10.1021/es00170a018, 1988.
- 371 Davidovits, P., Kolb, C. E., Williams, L. R., Jayne, J. T., and Worsnop, D. R.: Mass accommodation and  
372 chemical reactions at gas-liquid interfaces, *Chem. Rev.*, 106, 1323-1354, 10.1021/cr040366k, 2006.
- 373 Deister, U., and Warneck, P.: Photooxidation of sulfite (SO<sub>3</sub><sup>2-</sup>) in aqueous solution, *J. Phys. Chem.*, 94,  
374 2191-2198, 10.1021/j100368a084, 1990.
- 375 Eriksen, T. E.: pH Effects on the pulse radiolysis of deoxygenated aqueous solutions of sulphur dioxide, *Journal*  
376 *of the Chemical Society, Faraday Transactions 1: Physical Chemistry in Condensed Phases*, 70, 208-215,  
377 10.1039/f19747000208, 1974.
- 378 Gao, M., Carmichael, G. R., Wang, Y., Ji, D., Liu, Z., and Wang, Z.: Improving simulations of sulfate aerosols  
379 during winter haze over Northern China: the impacts of heterogeneous oxidation by NO<sub>2</sub>, *Front. Environ. Sci.*  
380 *Eng.*, 10, 16, 10.1007/s11783-016-0878-2, 2016.
- 381 Guo, H., Weber, R. J., and Nenes, A.: High levels of ammonia do not raise fine particle pH sufficiently to yield  
382 nitrogen oxide-dominated sulfate production, *Sci. Rep.*, 7, 12109, 10.1038/s41598-017-11704-0, 2017.
- 383 Hayon, E., Treinin, A., and Wilf, J.: Electronic spectra, photochemistry, and autoxidation mechanism of the  
384 sulfite-bisulfite-pyrosulfite systems. SO<sub>2</sub><sup>-</sup>, SO<sub>3</sub><sup>-</sup>, SO<sub>4</sub><sup>-</sup>, and SO<sub>5</sub><sup>-</sup> radicals, *J. Am. Chem. Soc.*, 94, 47-57,  
385 10.1021/ja00756a009, 1972.
- 386 He, H., Wang, Y., Ma, Q., Ma, J., Chu, B., Ji, D., Tang, G., Liu, C., Zhang, H., and Hao, J.: Mineral dust and  
387 NO<sub>x</sub> promote the conversion of SO<sub>2</sub> to sulfate in heavy pollution days, *Sci. Rep.*, 4, 10.1038/srep04172, 2014.
- 388 Herrmann, H.: Kinetics of aqueous phase reactions relevant for atmospheric chemistry, *Chem. Rev.*, 103,  
389 4691-4716, 10.1021/cr020658q, 2003.
- 390 Herrmann, H., Schaefer, T., Tilgner, A., Styler, S. A., Weller, C., Teich, M., and Otto, T.: Tropospheric  
391 Aqueous-Phase Chemistry: Kinetics, Mechanisms, and Its Coupling to a Changing Gas Phase, *Chem. Rev.*, 115,  
392 4259-4334, 10.1021/cr500447k, 2015.
- 393 Huang, L., Zhao, Y., Li, H., and Chen, Z.: Kinetics of Heterogeneous Reaction of Sulfur Dioxide on Authentic  
394 Mineral Dust: Effects of Relative Humidity and Hydrogen Peroxide, *Environ. Sci. Technol.*, 49, 10797-10805,  
395 10.1021/acs.est.5b03930, 2015.

396 Huie, R. E., and Neta, P.: Kinetics of one-electron transfer-reactions involving ClO<sub>2</sub> and NO<sub>2</sub>, *J. Phys. Chem.*,  
397 90, 1193-1198, 10.1021/j100278a046, 1986.

398 Huie, R. E., and Neta, P.: Rate constants for some oxidations of S(IV) by radicals in aqueous-solutions, *Atmos.*  
399 *Environ.*, 21, 1743-1747, 10.1016/0004-6981(87)90113-2, 1987.

400 Huie, R. E., Clifton, C. L., and Altstein, N.: A pulse radiolysis and flash photolysis study of the radicals SO<sub>2</sub>,  
401 SO<sub>3</sub>, SO<sub>4</sub> and SO<sub>5</sub>, *Radiat. Phys. Chem.*, 33, 361-370, 1989.

402 Huie, R. E.: Free radical chemistry of the atmospheric aqueous phase, in: *Progress and Problems in Atmospheric*  
403 *Chemistry*, WORLD SCIENTIFIC, 374-419, 1995.

404 Lee, Y.-N., and Schwartz, S. E.: Kinetics of oxidation of aqueous sulfur (IV) by nitrogen dioxide, in:  
405 *Precipitation Scavenging, Dry Deposition and Resuspension*, edited by: Pruppacher, H. R., Semonin, R. G., and  
406 Slinn, W. G. N., Elsevier, New York, 453-466, 1983.

407 Lelieveld, J., Gromov, S., Pozzer, A., and Taraborrelli, D.: Global tropospheric hydroxyl distribution, budget and  
408 reactivity, *Atmos. Chem. Phys.*, 16, 12477-12493, 10.5194/acp-16-12477-2016, 2016.

409 Li, H. J., Zhu, T., Zhao, D. F., Zhang, Z. F., and Chen, Z. M.: Kinetics and mechanisms of heterogeneous  
410 reaction of NO<sub>2</sub> on CaCO<sub>3</sub> surfaces under dry and wet conditions, *Atmos. Chem. Phys.*, 10, 463-474, 2010.

411 Littlejohn, D., Wang, Y. Z., and Chang, S. G.: Oxidation of aqueous sulfite ion by nitrogen-dioxide, *Environ. Sci.*  
412 *Technol.*, 27, 2162-2167, 10.1021/es00047a024, 1993.

413 Liu, M. X., Song, Y., Zhou, T., Xu, Z. Y., Yan, C. Q., Zheng, M., Wu, Z. J., Hu, M., Wu, Y. S., and Zhu, T.: Fine  
414 particle pH during severe haze episodes in northern China, *Geophys. Res. Lett.*, 44, 5213-5221,  
415 10.1002/2017gl073210, 2017.

416 Liu, Y. J., Zhu, T., Zhao, D. F., and Zhang, Z. F.: Investigation of the hygroscopic properties of Ca(NO<sub>3</sub>)(2) and  
417 internally mixed Ca(NO<sub>3</sub>)(2)/CaCO<sub>3</sub> particles by micro-Raman spectrometry, *Atmos. Chem. Phys.*, 8,  
418 7205-7215, 2008.

419 Ma, Q., He, H., Liu, Y., Liu, C., and Grassian, V. H.: Heterogeneous and multiphase formation pathways of  
420 gypsum in the atmosphere, *Phys. Chem. Chem. Phys.*, 15, 19196-19204, 10.1039/c3cp53424c, 2013.

421 Nakamoto, K.: *Infrared and Raman Spectra of Inorganic and Coordination Compounds Part A*, John Wiley  
422 & Sons, New York, 221-247 pp., 1997.

423 Nash, T.: Effect of nitrogen-dioxide and of some transition-metals on the oxidation of dilute bisulfite solutions,  
424 *Atmos. Environ.*, 13, 1149-1154, 10.1016/0004-6981(79)90038-6, 1979.

425 Pöschl, U., Rudich, Y., and Ammann, M.: Kinetic model framework for aerosol and cloud surface chemistry and  
426 gas-particle interactions - Part 1: General equations, parameters, and terminology, *Atmos. Chem. Phys.*, 7,  
427 5989-6023, 2007.

428 Podkrajšek, B., Grgić, I., and Turšič, J.: Determination of sulfur oxides formed during the S(IV) oxidation in the  
429 presence of iron, *Chemosphere*, 49, 271-277, [https://doi.org/10.1016/S0045-6535\(02\)00324-7](https://doi.org/10.1016/S0045-6535(02)00324-7), 2002.

430 Prinn, R. G., Huang, J., Weiss, R. F., Cunnold, D. M., Fraser, P. J., Simmonds, P. G., McCulloch, A., Harth, C.,  
431 Reimann, S., Salameh, P., O'Doherty, S., Wang, R. H. J., Porter, L. W., Miller, B. R., and Krummel, P. B.:  
432 Evidence for variability of atmospheric hydroxyl radicals over the past quarter century, *Geophys. Res. Lett.*, 32,  
433 10.1029/2004gl022228, 2005.

434 Santachiara, G., Prodi, F., and Vivarelli, F.: SO<sub>2</sub> oxidation in monodisperse droplets grown on carbon nuclei in  
435 presence of NO<sub>2</sub>, *J. Aerosol Sci.*, 21, S221-S224, 10.1016/0021-8502(90)90224-1, 1990.

436 Santachiara, G., Prodi, F., and Vivarelli, F.: Further experiments on SO<sub>2</sub> oxidation rate in monodisperse droplets  
437 grown on carbon nuclei in presence of O<sub>2</sub> and NO<sub>2</sub>, *J. Aerosol Sci.*, 24, 683-685,  
438 10.1016/0021-8502(93)90024-4, 1993.

439 Sarma, L. P., Prasad, P. S. R., and Ravikumar, N.: Raman spectroscopic study of phase transitions in natural  
440 gypsum, *J. Raman Spectrosc.*, 29, 851-856, 10.1002/(sici)1097-4555(199809)29:9<851::aid-jrs313>3.0.co;2-s,  
441 1998.

442 Seinfeld, J. H., and Pandis, S. N.: Atmospheric chemistry and physics: from air pollution to climate change, 2nd  
443 ed., John Wiley & Sons. Inc., 2006.

444 Shen, C. H., and Rochelle, G. T.: Nitrogen Dioxide Absorption and Sulfite Oxidation in Aqueous Sulfite, *Environ.*  
445 *Sci. Technol.*, 32, 1994-2003, 10.1021/es970466q, 1998.

446 Shi, X. L.: Generation of SO<sub>3</sub><sup>-</sup> and OH radicals in SO<sub>3</sub><sup>2-</sup> reactions with inorganic environmental-pollutants and its  
447 implications to SO<sub>3</sub><sup>2-</sup> toxicity, *J. Inorg. Biochem.*, 56, 155-165, 10.1016/0162-0134(94)85002-x, 1994.

448 Spindler, G., Hesper, J., Brüggemann, E., Dubois, R., Müller, T., and Herrmann, H.: Wet annular denuder  
449 measurements of nitrous acid: laboratory study of the artefact reaction of NO<sub>2</sub> with S(IV) in aqueous solution  
450 and comparison with field measurements, *Atmos. Environ.*, 37, 2643-2662, 10.1016/s1352-2310(03)00209-7,  
451 2003.

452 Turšič, J., Grgić, I., and Bizjak, M.: Influence of NO<sub>2</sub> and dissolved iron on the S(IV) oxidation in synthetic  
453 aqueous solution, *Atmos. Environ.*, 35, 97-104, [https://doi.org/10.1016/S1352-2310\(00\)00283-1](https://doi.org/10.1016/S1352-2310(00)00283-1), 2001.

454 Wang, G., Zhang, R., Gomez, M. E., Yang, L., Levy Zamora, M., Hu, M., Lin, Y., Peng, J., Guo, S., Meng, J., Li,  
455 J., Cheng, C., Hu, T., Ren, Y., Wang, Y., Gao, J., Cao, J., An, Z., Zhou, W., Li, G., Wang, J., Tian, P.,  
456 Marrero-Ortiz, W., Secret, J., Du, Z., Zheng, J., Shang, D., Zeng, L., Shao, M., Wang, W., Huang, Y., Wang, Y.,  
457 Zhu, Y., Li, Y., Hu, J., Pan, B., Cai, L., Cheng, Y., Ji, Y., Zhang, F., Rosenfeld, D., Liss, P. S., Duce, R. A., Kolb,  
458 C. E., and Molina, M. J.: Persistent sulfate formation from London Fog to Chinese haze, *Proc. Nat. Acad. Sci.*  
459 *U.S.A.*, 113, 13630-13635, 10.1073/pnas.1616540113, 2016.

460 Waygood, S. J., and McElroy, W. J.: Spectroscopy and decay kinetics of the sulfite radical anion in aqueous  
461 solution, *J. Chem. Soc.-Faraday Trans.*, 88, 1525-1530, 10.1039/ft9928801525, 1992.

462 Xue, J., Yuan, Z. B., Griffith, S. M., Yu, X., Lau, A. K. H., and Yu, J. Z.: Sulfate Formation Enhanced by a  
463 Cocktail of High NO<sub>x</sub>, SO<sub>2</sub>, Particulate Matter, and Droplet pH during Haze-Fog Events in Megacities in China:  
464 An Observation-Based Modeling Investigation, *Environ. Sci. Technol.*, 50, 7325-7334, 10.1021/acs.est.6b00768,  
465 2016.

466 Zhang, J. K., Sun, Y., Liu, Z. R., Ji, D. S., Hu, B., Liu, Q., and Wang, Y. S.: Characterization of submicron  
467 aerosols during a month of serious pollution in Beijing, 2013, *Atmos. Chem. Phys.*, 14, 2887-2903,  
468 10.5194/acp-14-2887-2014, 2014.

469 Zhao, D., Song, X., Zhu, T., Zhang, Z., and Liu, Y.: Multiphase Reaction of SO<sub>2</sub> with NO<sub>2</sub> on CaCO<sub>3</sub> Particles.  
470 1. Oxidation of SO<sub>2</sub> by NO<sub>2</sub>, *Atmos. Chem. Phys. Discuss.*, 2017, 1-23, 10.5194/acp-2017-610, 2017.

471 Zhao, D. F., Zhu, T., Chen, Q., Liu, Y. J., and Zhang, Z. F.: Raman micro-spectrometry as a technique for  
472 investigating heterogeneous reactions on individual atmospheric particles, *Sci. China Chem.*, 54, 154-160,  
473 10.1007/s11426-010-4182-x, 2011.

474 Zheng, B., Zhang, Q., Zhang, Y., He, K. B., Wang, K., Zheng, G. J., Duan, F. K., Ma, Y. L., and Kimoto, T.:  
475 Heterogeneous chemistry: a mechanism missing in current models to explain secondary inorganic aerosol  
476 formation during the January 2013 haze episode in North China, *Atmos. Chem. Phys.*, 15, 2031-2049,  
477 10.5194/acp-15-2031-2015, 2015a.

478 Zheng, G. J., Duan, F. K., Su, H., Ma, Y. L., Cheng, Y., Zheng, B., Zhang, Q., Huang, T., Kimoto, T., Chang, D.,  
479 Poschl, U., Cheng, Y. F., and He, K. B.: Exploring the severe winter haze in Beijing: the impact of synoptic  
480 weather, regional transport and heterogeneous reactions, *Atmos. Chem. Phys.*, 15, 2969-2983,  
481 10.5194/acp-15-2969-2015, 2015b.

482 Zhu, T., Shang, J., and Zhao, D. F.: The roles of heterogeneous chemical processes in the formation of an air  
483 pollution complex and gray haze, *Sci. China Chem.*, 54, 145-153, 10.1007/s11426-010-4181-y, 2011.

484

485

486

487

**Table 1.** Reactive uptake coefficient of SO<sub>2</sub> for sulfate formation at 82% RH and at different O<sub>2</sub> concentrations.

SO <sub>2</sub> /NO <sub>2</sub> /O <sub>2</sub> concentration	$\gamma$
75 ppm/ 75 ppm/ 86 %	$1.7 \times 10^{-5}$
75 ppm/ 75 ppm/ 20 %	$1.2 \times 10^{-5}$
75 ppm/ 75 ppm/ 5 %	$3.5 \times 10^{-6}$

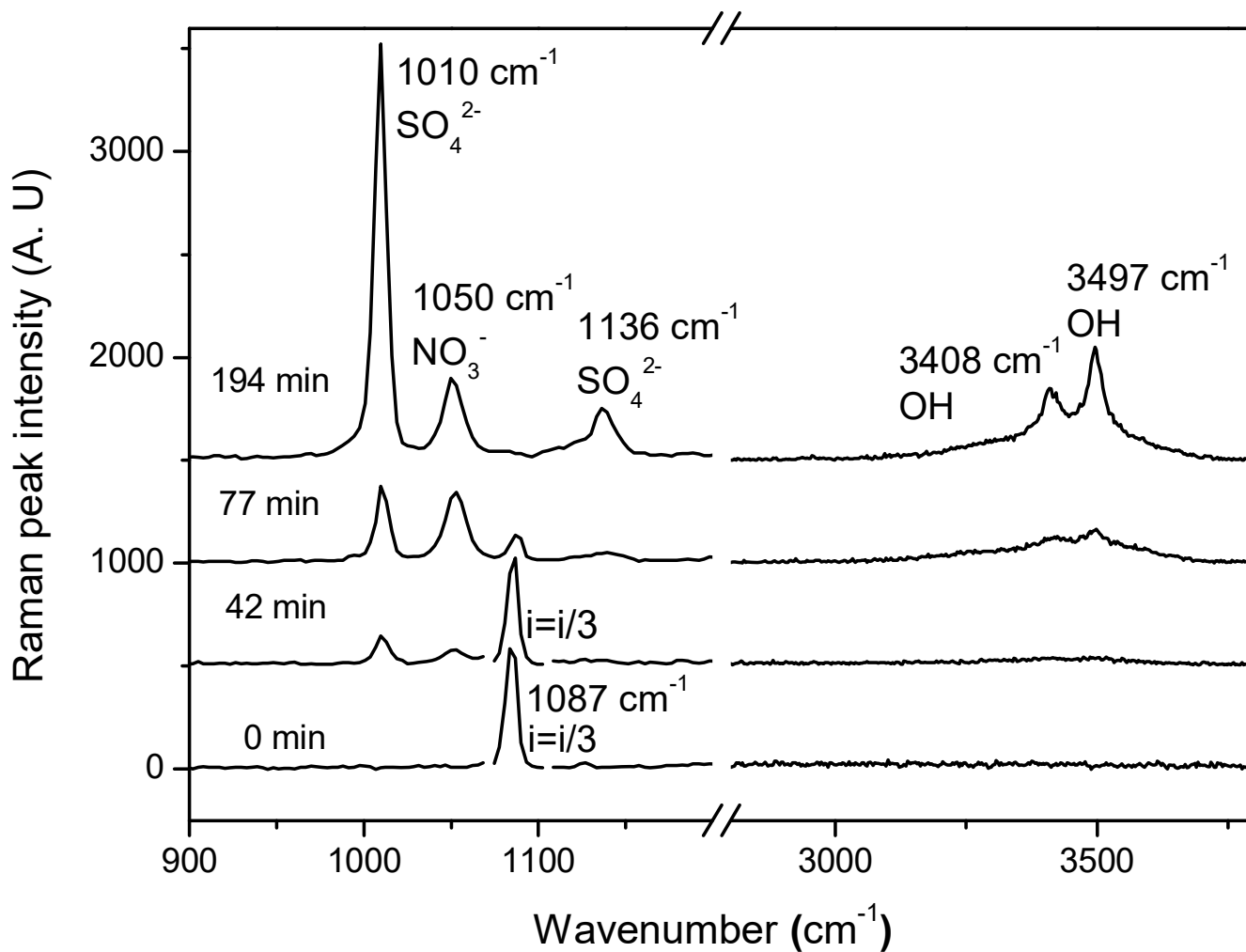
488  
489

490

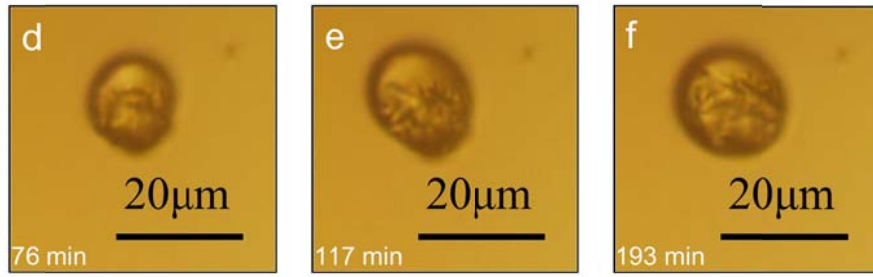
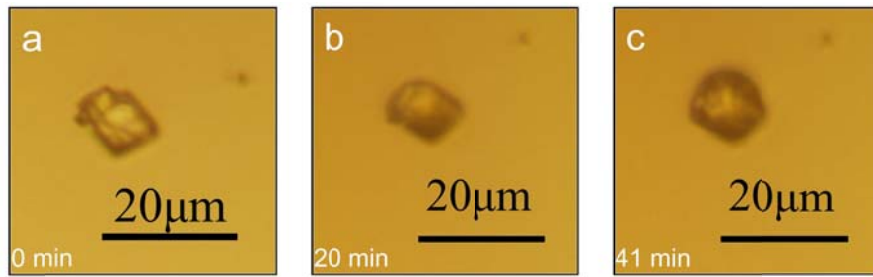
**Table 2.** Summary of the mechanism of the reaction S(IV) with O<sub>2</sub>/NO<sub>2</sub>

Step	Reactions
Initiation	$\text{NO}_2(\text{aq}) + \text{HSO}_3^-(\text{aq}) \rightarrow \text{NO}_2^-(\text{aq}) + \text{SO}_3^{\bullet-}(\text{aq}) + \text{H}^+(\text{aq})$ (R8)
Propagation	$\text{SO}_3^{\bullet-}(\text{aq}) + \text{O}_2(\text{aq}) \rightarrow \text{SO}_5^{\bullet-}(\text{aq})$ (R12)
	$\text{SO}_5^{\bullet-}(\text{aq}) + \text{HSO}_3^-(\text{aq}) \rightarrow \text{HSO}_5^-(\text{aq}) + \text{SO}_3^{\bullet-}(\text{aq})$ (R13)
	$\text{HSO}_5^-(\text{aq}) + \text{HSO}_3^-(\text{aq}) \rightarrow 2\text{SO}_4^{2-}(\text{aq}) + 2\text{H}^+(\text{aq})$ (R14)
	$\text{SO}_5^{\bullet-}(\text{aq}) + \text{HSO}_3^-(\text{aq}) \rightarrow \text{SO}_4^{2-}(\text{aq}) + \text{SO}_4^{\bullet-}(\text{aq}) + \text{H}^+(\text{aq})$ (R15)
	$\text{SO}_4^{\bullet-}(\text{aq}) + \text{HSO}_3^-(\text{aq}) \rightarrow \text{SO}_4^{2-}(\text{aq}) + \text{SO}_3^{\bullet-}(\text{aq}) + \text{H}^+(\text{aq})$ (R16)
Termination	$\text{SO}_3^{\bullet-}(\text{aq}) + \text{SO}_3^{\bullet-}(\text{aq}) \rightarrow \text{S}_2\text{O}_6^{2-}(\text{aq})$ (R9)
	$\text{SO}_3^{\bullet-}(\text{aq}) + \text{SO}_3^{\bullet-}(\text{aq}) \rightarrow \text{SO}_3^{2-}(\text{aq}) + \text{SO}_3$ (R10)
	$\text{SO}_3(\text{aq}) + \text{H}_2\text{O} \rightarrow \text{SO}_4^{2-}(\text{aq}) + 2\text{H}^+(\text{aq})$ (R11)
	$\text{SO}_4^{\bullet-}(\text{aq}) + \text{SO}_4^{\bullet-}(\text{aq}) \rightarrow \text{S}_2\text{O}_8^{2-}(\text{aq})$ (R17)
	$\text{SO}_5^{\bullet-}(\text{aq}) + \text{SO}_5^{\bullet-}(\text{aq}) \rightarrow \text{S}_2\text{O}_8^{2-}(\text{aq}) + \text{O}_2(\text{aq})$ (R18)

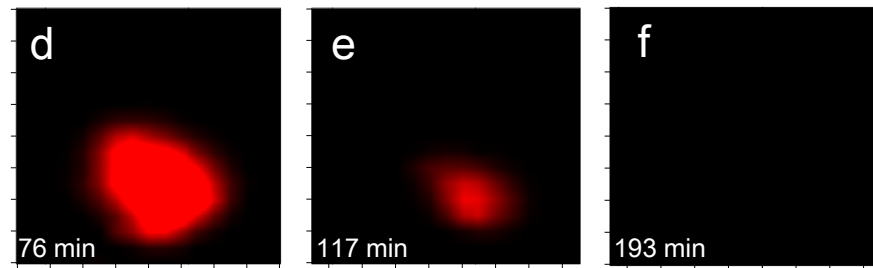
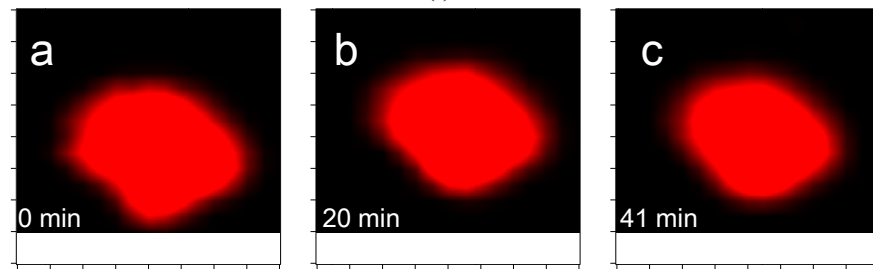




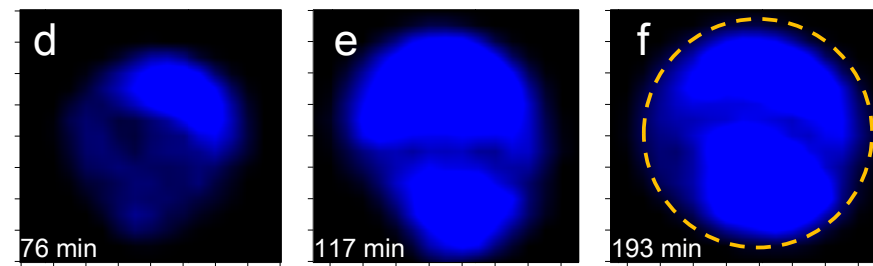
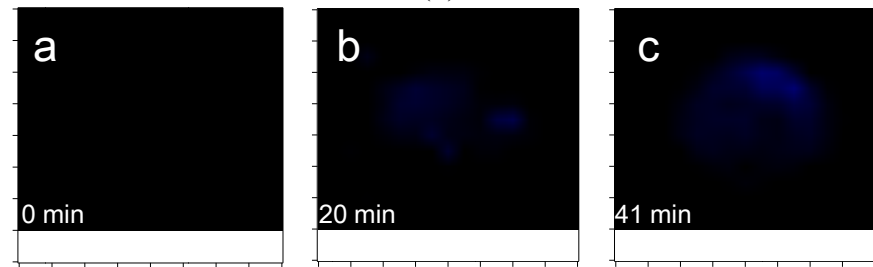
493  
 494 Figure 1. Raman spectra of a  $\text{CaCO}_3$  particle during the multiphase reaction of  $\text{SO}_2$  with  $\text{O}_2/\text{NO}_2/\text{H}_2\text{O}$   
 495 on the particle.  $\text{SO}_2$ : 75 ppm,  $\text{NO}_2$ : 75 ppm, RH: 72%,  $\text{O}_2$ : 20%. The peak intensity of carbonate (1087  
 496  $\text{cm}^{-1}$ ) at 0 and 42 min was divided by three for clarity.  
 497



(i)



(ii)

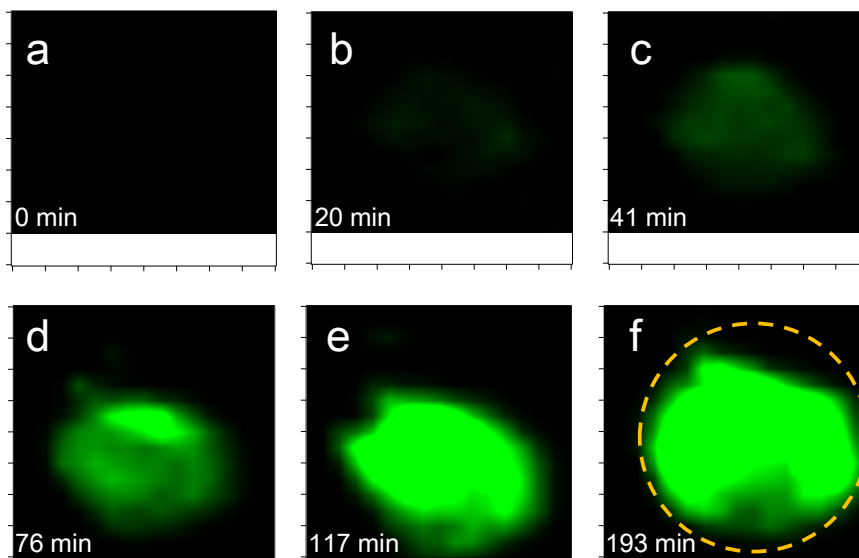


(iii)

498  
499

500  
501

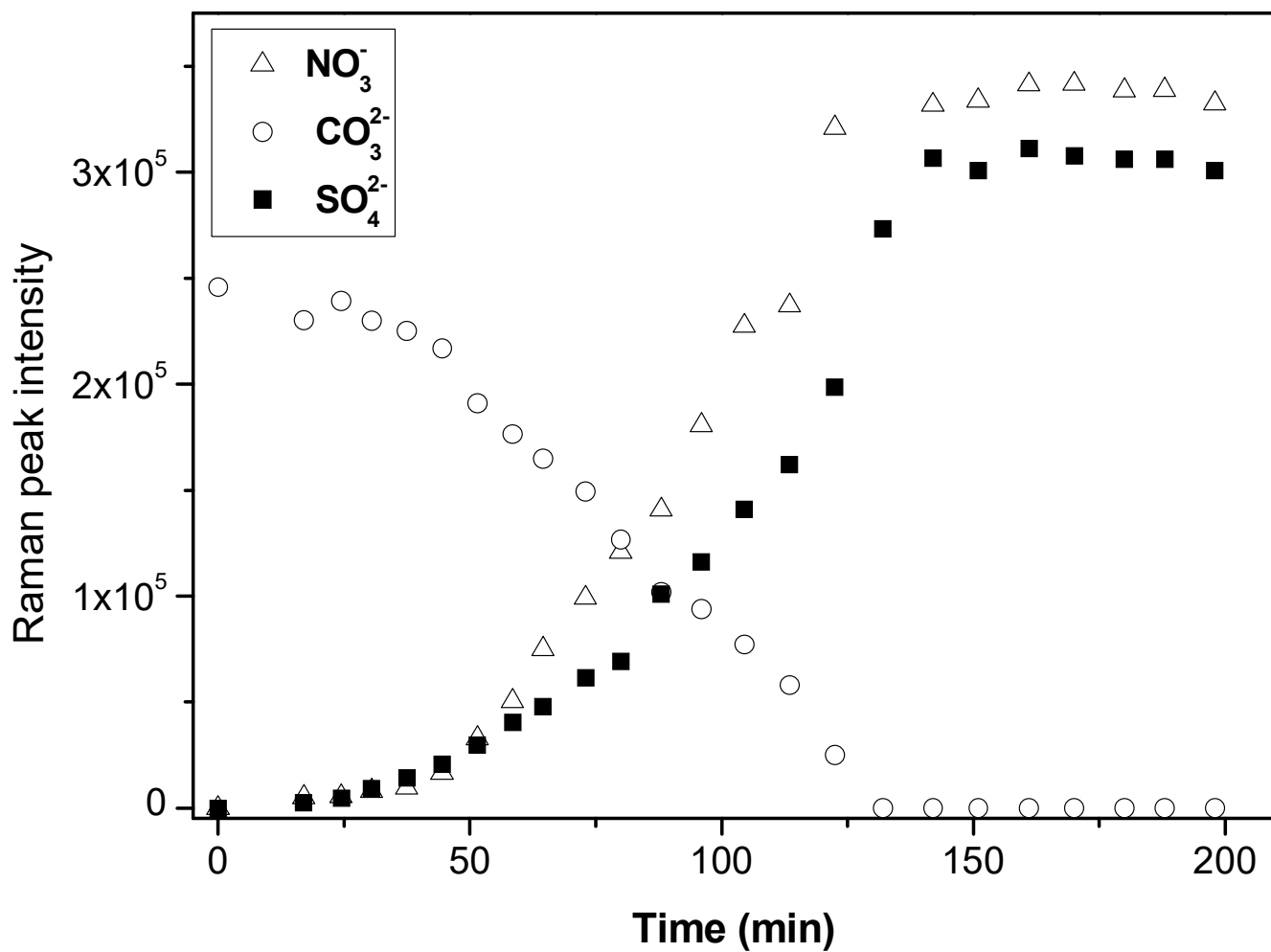
502  
503



504  
505  
506  
507  
508  
509  
510  
511  
512  
513

(iv)

Figure 2. Microscopic image (i) and Raman mapping image of carbonate (ii), nitrate (iii), and sulfate (iv) on the  $\text{CaCO}_3$  particle during the multiphase reaction  $\text{SO}_2$  with  $\text{O}_2/\text{NO}_2/\text{H}_2\text{O}$  on the particle. A-f corresponds to the reaction time of 0, 20, 41, 76, 117, and 193 min.  $\text{SO}_2$ : 75 ppm,  $\text{NO}_2$ : 75 ppm, RH: 72%,  $\text{O}_2$ : 20%. The mapping image of carbonate, nitrate, and sulfate are made using the peak area at 1050, 1010, and 1087  $\text{cm}^{-1}$ , respectively. The red, blue, and green colors indicate the peak intensity of carbonate, nitrate, and sulfate, respectively. The dashed lines in panel iii-f and iv-f indicate the shape of the droplet at the end of the reaction.



514

515 Figure 3. Time series of the Raman peak intensity of NO<sub>3</sub><sup>-</sup>, SO<sub>4</sub><sup>2-</sup>, and CO<sub>3</sub><sup>2-</sup> during the reaction of SO<sub>2</sub>  
 516 with O<sub>2</sub>/NO<sub>2</sub>/H<sub>2</sub>O on CaCO<sub>3</sub> particles. SO<sub>2</sub>: 75 ppm, NO<sub>2</sub>: 75 ppm, RH: 72%, O<sub>2</sub>: 20%. The intensity of  
 517 NO<sub>3</sub><sup>-</sup>, SO<sub>4</sub><sup>2-</sup>, and CO<sub>3</sub><sup>2-</sup> show the peak area at 1050, 1010, and 1087 cm<sup>-1</sup>, respectively, in Raman spectra  
 518 obtained by Raman mapping.

519

520